

A Simple 1-D Physical Model for the Crawling Nematode Sperm Cell

A. Mogilner¹ and D. W. Verzi²

Received January 30, 2002; accepted August 7, 2002

We develop a one-dimensional physical model of the crawling movement of simple cells: The sperm of a nematode, *Ascaris suum*. The model is based on the assumptions that polymerization and bundling of the cytoskeletal filaments generate the force for extension at the front, and that energy stored in the gel formed from the filament bundles is subsequently used to produce the contraction that pulls the rear of the cell forward. The model combines the mechanics of protrusion and contraction with chemical control, and shows how their coupling generates stable rapid migration, so that the cell length and velocity regulate to constant values.

KEY WORDS: Cell movements; biophysical model; Brownian Ratchet; entropic contraction.

1. INTRODUCTION

Understanding the mechanics of cell crawling has important implications for cancer cell metastasis, skin fibroblast migration in wound healing, white blood cell locomotion during tissue inflammation, and a host of other medical and biological applications. It is fascinating to observe cells crawling in the laboratory, as they seem to glide effortlessly across a glass surface, maintaining their overall shape.⁽¹⁾ Many cells accomplish this smooth motion by developing a motile appendage (*lamellipod*) in front of the cell body (Fig. 1). The cell body contains the nucleus and organelles, while the lamellipod is filled with complex and dynamic protein networks. Mechanically, the cell body is but a passive cargo, while the lamellipod

¹ Department of Mathematics, University of California, One Shields Ave., Davis, California 95616; e-mail: mogilner@math.ucdavis.edu

² Department of Mathematics, San Diego State University-Imperial Valley, Calexico, California 92231.

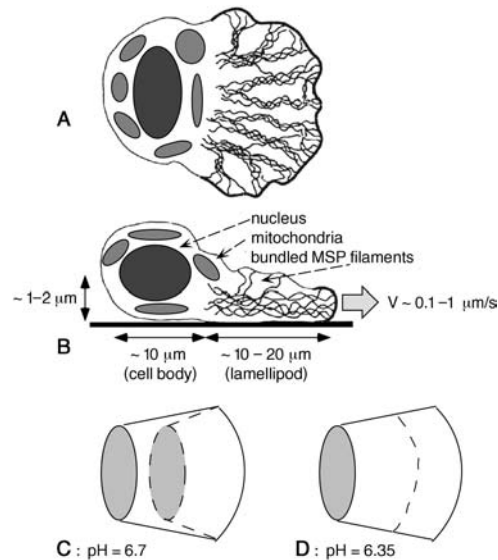


Fig. 1. Nematode sperm cell: (A) A schematic top view: Nucleus and mitochondria are at the rear (left in the figure). Flat and wide lamellipod at the front is filled with bundles of MSP filaments extending radially from the cell body. The bundles are connected with each other by free MSP filaments; (B) A schematic side view for the crawling cell; (C) When external pH is lowered to 6.7, the leading edge (solid arch) stops moving, while the cell body (shaded ellipsoid) continues to advance. Dashed parts of the figure show positions of the cell body and lamellipodial lateral sides at a later time; (D) When external pH is lowered to 6.35, the forward translocation of the cell body stops, but the leading edge of the MSP network is pulled backward. The solid and dashed arches show the position of the cell front at earlier and later time, respectively.

is the engine that moves the cell.⁽²⁾ Chemically, the cell body plays an important part in the regulation of these movements.

Roughly speaking, cell migration can be dissected into five consecutive steps.⁽³⁾ First, the lamellipodial protein network grows at the leading edge forming a *protrusion*. Then, firm *adhesion* to the surface upon which the cell crawls must take place at the front. Thirdly, *contraction* forces develop within the lamellipod; then adhesion to the surface weakens in the vicinity of the cell body and rear part of the lamellipod. Finally, the forces of contraction within the lamellipod pull the cell body forward. The prevalent belief in cell biology is that there are three basic processes: protrusion at the front, contraction at the rear, and graded adhesion, all acting in concert to accomplish rapid and stable cell migration.⁽⁴⁾

In most crawling cells, the main mechanical “players” in the lamellipod are the proteins actin and myosin.⁽⁴⁾ Actin forms polar fibers that grow at the front of the cell and shrink at the rear, and myosin molecular motors

pull the cell body forward using polarized actin filaments as “tracks.”^(5,6) Actin-myosin networks are very heterogeneous and anisotropic. They are involved in many different aspects of cell behavior and require a host of accessory proteins. This complexity has frustrated interpretation of many experiments. Because of that, simple and specialized cells, like the sperm of a nematode (*Ascaris suum*), have attracted the attention of experimentalists working on cell motility.⁽⁷⁾

Nematode sperm cells crawl, rather than swim, like most other sperm cells. The crawling cells, moving at tenths of microns per second, are tens of microns long and wide and a few microns high; see Fig. 1. In these cells, which appear to be dedicated solely to migration, the locomotion machinery has been dramatically simplified. Nematode sperm cells discard actin and most organelles (only the nucleus and mitochondria are left) after meiosis. They move using a very basic mechanical engine based upon the lamellipodial network consisting of *major sperm protein* (MSP). Importantly, these cells look and move much like similarly shaped actin based cells. Understanding locomotion of the sperm cells will elucidate the general principles of migration in actin based cells.

Major sperm protein forms *symmetric, hydrophobic and basic dimers*, which diffuse freely in the *cytoplasm*. Dimers polymerize into helical sub-filaments, which wind together to form larger *filaments*.⁽⁷⁻⁹⁾ MSP polymers can spontaneously assemble into higher-ordered *fiber complexes* or *bundles*. The same interaction interfaces (hydrophobic patches) that are employed to assemble sub-filaments into polymers are thought to be responsible for this bundling. Twenty to thirty branched, densely packed bundles intertwined with unbundled filaments span the lamellipod from the leading edge to the rear where they join the cell body (see Fig. 1).

Filaments assemble and bundle into fiber complexes along the leading edge and disassemble at the rear of the lamellipod.⁽⁷⁻⁹⁾ This *treadmilling* process (assembly at the front and disassembly at the rear create forward translocation of the structure, though there is no movement in the middle) is at the core of the cell migration phenomenon. Because of the symmetric structure of MSP dimers, the polymers have no overall structural polarity, so molecular motors are unlikely to be responsible for the movements. Generally speaking, two questions are central for understanding the mechanics of locomotion: what is the nature of the forces of protrusion and contraction, and how these forces are regulated in space and time to achieve steady, stable movement?

The following experimental observations give clues to the answers. A proximal-distal pH gradient of ≈ 0.2 pH units is maintained in the steadily moving cell: at the rear of the lamellipod pH ≈ 6.0 , while at the front pH ≈ 6.2 .⁽¹⁰⁾ The origin of this gradient is unknown, but it is probably

a source of protons from the mitochondria in the cell body. When pH in the external solution is lowered from 7 to 6.7, the protrusion at the leading edge stops, while the cell body continues to advance. When the external pH is lowered further to 6.35, the cell body stops advancing, and the leading edge is pulled back⁽⁸⁾ (Fig. 1). *In vitro* experiments confirm that MSP assembly and filament bundling take place at higher pH, while un-bundling and disassembly occur at lower pH.⁽⁹⁾ Examination of crawling sperm by interference reflection microscopy has revealed that the adhesive sites are located primarily in the lamellipod, with few if any in the cell body. The pattern of adhesion appears nearly constant across the front and middle of the lamellipod to the transition region in the rear, so that the strength of adhesion appears to be nearly a “step” function. The hypothesis is that the pH regulates adhesion: attachment to the surface is firm at high pH and weak at low pH.

These observations lead to the following qualitative “push-pull” model:⁽⁷⁾

- (i) The cell body maintains a pH gradient across the lamellipod.
- (ii) Filament assembly and bundling take place predominantly in the more basic environment of the distal region near the cell front, leading to protrusion at the front.
- (iii) Filament disassembly and un-bundling take place predominantly in the more acidic environment of the proximal region near the cell body, causing contraction at the rear.
- (iv) The protrusion at the front and contraction at the rear are separated spatially by firm adhesion at the front and middle of the lamellipod, and weak or non-existent adhesion at the rear, leading to forward translocation of the entire cell.

Without a physical model, the “push-pull” hypothesis remains a mere cartoon. A quantitative model is required to examine whether the suggested coupling of biophysical and regulation mechanisms can account for observed dimensions and rates of motion of the cell. Bottino *et al.*⁽¹⁰⁾ have developed a quantitative, two dimensional model of the crawling cell which considers the lamellipod as a flat, dynamic domain. Simulations using a finite elements method produce stable moving shapes resembling those of the motile cells. However, computer simulations of two-dimensional models are time consuming, which prohibits simulation of the polymer bundles. Rather, Bottino *et al.* modelled the lamellipodial network as an isotropic elastic plate with moving boundaries.

In this paper, we construct a “minimal,” one-dimensional physical model of the sperm cell, using the same assumptions about the mechanochemistry of the lamellipod as Bottino *et al.* Essentially, this is the model of one lamellipodial bundle running the length of the cell, from the rear to the front. By simplifying the geometry in the model, simulations are relatively fast and easy to perform, and the results are easier to interpret. This enables us to consider the lamellipodial mechanics in greater detail, which sheds light on basic physical processes in the moving cell.

In the next section we discuss the physical processes underlying the phenomenon of locomotion. Based on this discussion, we derive conservation laws and constitutive relations governing lamellipodial mechanics in Section 3. We present the results of model’s simulations in Section 4 and discuss their biological implications in Section 5. Details of the analysis of the model are reported in the Appendix.

2. PHYSICAL MODEL

The model describes explicitly only the lamellipod–cytoskeletal strip. The cell body in the model is mechanically passive, though chemically it plays an important role. The qualitative physical idea of the model is as follows.

Protrusion. MSP polymerizes into filaments at the leading edge. Consider a filament incorporated into the bundle. The filament’s tip is growing at a rate V_p . Hydrophobic patches are located periodically at the sides of the filament. Successive adhesive interactions between the growing filament and other filaments in the bundle “lock” the growing filament in an almost straight configuration. This spontaneous bundling forces the filaments to assume an end-to-end distance, which is larger than it was in solution. That is, the enthalpic part of the free energy of assembly dominates the entropy loss accompanying lateral association, so that filaments are held in a ‘stretched’ configuration. Thus, each bundle of filaments “stores” the elastic energy of its constituent filaments, and is stiffer.

At the same time, free filament tips ahead of the most advanced hydrophobic patch are undulating thermally, so that the distance from the most advanced hydrophobic patch to the cell membrane is generally shorter than the length of the free filament tips. However, when a tip grows so long that another hydrophobic patch appears at the front, that tip binds to the bundle, causing leading edge extension (Fig. 2). Thus, the bundling process “ratchets” forward the thermal bending of individual filaments. In Appendix A, we show that this “bundling ratchet” is capable of generating

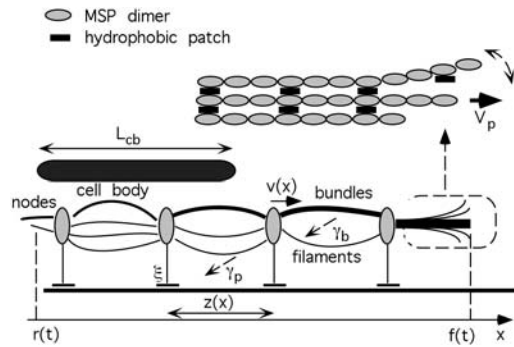


Fig. 2. A side view of the physical 1-D model of the treadmilling MSP bundle. $x = f(t)$ and $x = r(t)$ are the coordinates of the front and rear of the cell, respectively, in the laboratory coordinate system. Shaded ellipsoids show “cytoskeletal nodes” that attach to the surface through the effective sliding frictional elements, characterized by the effective drag coefficient $\zeta(x)$. The nodes move with velocity $v(x)$, which is a function of node position. The MSP bundles (thick) between the nodes are in compression. Filaments unbundle with rate γ_b . Individual filaments (thin) are under tension: they attempt to contract. They disassemble with rate γ_p . Insert: MSP filaments grow at the rate V_p . Undulating tips bind to the bundled filaments, straightening and generating the force of protrusion.

a protrusive force strong enough to maintain an effective growth rate of the bundle that is equal to the polymerization velocity of individual filaments.

Contraction. At the rear of the cell, where the cytoplasm is more acidic, hydrophobic adhesion weakens,⁽¹⁰⁾ and the unbundling process is triggered. As individual filaments disassociate from the bundle, they attempt to contract entropically to their equilibrium end-to-end length, acting effectively as springs in series (Fig. 2). We assume the existence of “cytoskeletal nodes”: local aggregates of MSP fibers which adhere to the surface. These nodes play an important mechanical role: the ends of local bundles and individual filaments attach to these nodes.³ The free energy of bundling that was supplied to the system at the front is released, generating a contractile stress. Following unbundling and subsequent entropic contraction, the filaments are depolymerized (both under the cell body, and more rapidly at the rear end of the cell with the rate V_d), and MSP dimers spread over the cytoplasm by diffusion.

Adhesion. We further propose (following ref 10) that adhesion of the lamellipodium to the substratum also decreases in the acidic environment at the rear of the cell. Thus the generated contractile stress pulls the cell body forward, rather than pulling the leading edge back.

³The structure of our model is analogous to a muscle sarcomere: Nodes play the role of Z-discs, while MSP bundles function similarly to contracting actin-myosin bundles.⁽¹⁾

Biochemical Regulation. The precise role played by pH in MSP turnover, bundling and adhesion is yet to be established. In the model, we use pH *distribution* as a marker for these processes. We assume that protons constantly appear at the cell body, and that protons leak out from the lamellipod, maintaining a gradient of proton concentration in the lamellipod. We investigate this pH distribution quantitatively in Appendix B. We introduce phenomenological pH dependencies of unbundling and depolymerization rates, based upon observations that filaments disassociate from each other and disassemble at low pH.

Adhesion of MSP filaments to the cell membrane, and adhesion of the cell membrane to the surface seem to have an electrostatic character: Basic MSP fibers carry a net positive charge. They are attracted to the inner leaflet of the plasma membrane, which carries negatively charged lipids. The lipid mobile positive charges on the outer membrane leaflet, in turn, are attracted to the negatively charged glass coverslip. The physics of this interaction is discussed in more detail in ref. 10. In the model, we assume that adhesion between the cytoskeleton and the membrane is a function of pH, such that lowering the pH disrupts adhesion.⁽⁸⁾

Two factors regulate the rate of MSP assembly at the front. First, this rate is controlled by pH: MSP assembly is fast at high pH, and vanishes at low pH. Second, a membrane protein acts in conjunction with at least two soluble cytoplasmic proteins to facilitate local MSP polymerization. As the cell becomes longer, the constant total amount of available membrane protein must be dispersed over a larger lamellipodial surface. The resulting decrease concentration of membrane protein slows down of the rate of MSP assembly. Effectively, this assembly rate is a decreasing function of cell length.

Note, that the model needs a biochemical “indicator” of distance from the leading edge for control of cytoskeletal processes. Moreover, a feedback control loop through which the front is prevented from running away from the back, or the back from catching up with the front, is needed. We draft the pH gradient and depletion of membrane regulatory proteins to play this role, because few experimental observations show that the pH gradient exists, and that pH influences the processes of assembly, disassembly, contraction and adhesion. However, there is no proof that the pH gradient is the only regulator. Other factors, such as membrane tension and turnover of MSP monomers, can play this role.

3. MODEL EQUATIONS

Geometry of the Model. Model variables and parameters are listed in Tables I and II, respectively. Effectively, we model one long bundle

Table I. Model Variables

Symbol	Definition	Units
x	Coordinate in the laboratory coordinate system	[μm]
y	Distance between cytoskeletal point and cell rear	[μm]
t	Time	[s]
$r(t)$	Coordinate of the cell rear	[μm]
$f(t)$	Coordinate of the cell front	[μm]
$b(x, t)$	Length density of bundled polymers	[$\mu\text{m}/\mu\text{m}$]
$p(x, t)$	Length density of free polymers	[$\mu\text{m}/\mu\text{m}$]
$c(x, t)$	Density of cytoskeletal nodes	[$1/\mu\text{m}$]
$v(x, t)$	Cytoskeletal velocity	[$\mu\text{m}/\text{s}$]
$\gamma_b(x, t)$	Rate of unbundling	[1/s]
$\gamma_p(x, t)$	Rate of disassembly	[1/s]
$\xi(x, t)$	Effective drag coefficient	[$\text{pN} \cdot \text{s}/\mu\text{m}^2$]
$V_p(t)$	Rate of polymerization at the front	[$\mu\text{m}/\text{s}$]

stretching from the front to the rear of the cell, composed of many bundled MSP filaments. Thus, the model is one-dimensional; x is the coordinate of cytoskeletal elements in the laboratory coordinate system, and the x -axis is oriented in the direction of cell migration. In this coordinate system, we denote the dynamic positions of the cell front and rear as $f(t)$ and $r(t)$, respectively (Fig. 2). We model the cell body by the segment of length $L_{\text{cb}} = 10 \mu\text{m}$ and assume that the cell body “sits on top” of the bundle at

Table II. Model Parameters

Symbol	Definition	Dimensional units	Dimensionless units
L_{cb}	Cell body length	10 μm	1
L	Distance from the rear to the critical pH level	11 μm	1
γ_b	Rate of unbundling	0.175/s	7.0
α_p	Rate of depolymerization	0.025/s	1.0
β_p	Rate of depolymerization	0.0225/s	0.9
α_ξ	Drag coefficient	70 $\text{pN} \cdot \text{s}/\mu\text{m}^2$	17.5
β_ξ	Drag coefficient	50 $\text{pN} \cdot \text{s}/\mu\text{m}^2$	12.5
V_0	Rate of MSP assembly	3.2 $\mu\text{m}/\text{s}$	12.8
η	Rate of change in space	1/ μm	10
ρ	Rest length of the bundle	1 μm	0.1
κ	Effective spring constant of the free filament	1 $\text{pN}/\mu\text{m}$	1
K	Effective spring constant of the bundled filament	1 $\text{pN}/\mu\text{m}$	1
b_0	Leading edge density of the bundled filaments	500 $\mu\text{m}/\mu\text{m}$	500
V_d	Rate of disassembly at the rear	1.25 $\mu\text{m}/\text{s}$	5

the rear of the cell (unpublished observations, T. Roberts). Three densities—cytoskeletal nodes density, $c(x, t)$ [$\#/\mu\text{m}$], and length densities of bundled and free polymers (filaments), $b(x, t)$ and $p(x, t)$ [$\mu\text{m}/\mu\text{m}$], respectively—describe the dynamics of the cell.⁴

Conservation Laws. The following conservation laws govern lamellipodial dynamics:

$$\frac{\partial b}{\partial t} = -\frac{\partial}{\partial x}(vb) - \gamma_b(y)b, \quad (1)$$

$$\frac{\partial p}{\partial t} = -\frac{\partial}{\partial x}(vp) + \gamma_b(y)b - \gamma_p(y)p, \quad (2)$$

$$\frac{\partial c}{\partial t} = -\frac{\partial}{\partial x}(vc). \quad (3)$$

The first terms in the right-hand-sides of these equations describe cytoskeletal drift with rate $v(x, t)$ (Fig. 2). The second terms in the right-hand-sides of Eqs. (1) and (2) are responsible for unbundling of filaments with rate $\gamma_b(y)$, which is a function of distance from the rear of the cell, $y = x - r(t)$ (see Appendix B). The third term in the right-hand-side of Eq. (2) describes the filament disassembly with rate $\gamma_p(y)$.

Lamellipodial Mechanics. The distance between the ends of individual filaments is equal to the distance between the neighboring cytoskeletal nodes, $z(x)$ (Fig. 2). Flexible filament, the ends of which are separated by distance z , acts as an effective linear spring.⁽¹¹⁾ The entropic force of contraction pulling these ends together is equal to κz , where κ is the effective spring constant of an individual filament. (We estimate the values of model parameters in Appendix C and Table II.) The rest length of this effective spring is equivalent to the equilibrium length of an individual filament and is approximately equal to zero, if the filament's persistence length is much less, than its contour length (see Appendix).

Parts of the bundle located between neighboring cytoskeletal nodes are also modeled as an effective linear spring, though the origin of this spring force is elastic, rather than entropic, as in the case of an individual filament. Indeed, large numbers (hundreds) of bundled filaments make the bundle rigid. The corresponding spring constant scales as the number of bundled filaments (or as the crosssectional area),⁽¹²⁾ so that the force generated by a bundle spring is equal to $Kb(z - \rho)$, where ρ is the corresponding

⁴ Polymer densities may be thought of as either the total length of polymers per unit length, or as the number of polymers passing through a point.

rest length, which we assume to be constant. K is the corresponding proportionality coefficient.

In one dimension, the total stress is computed as the sum of these two spring forces. Taking into account the relation between inter-node distance and node density, $z(x) = 1/c(x)$, we can write the expression for cytoskeletal stress in the form:

$$\sigma(x, t) = Kb(x, t) \left(\frac{1}{c(x, t)} - \rho \right) + \kappa p(x, t) \frac{1}{c(x, t)}. \quad (4)$$

In a continuous model, the force on cytoskeletal nodes is equal to the gradient of the stress. We model adhesion with the sliding friction elements associated with cytoskeletal nodes (Fig. 2), such that node velocity is proportional to the force applied to the node. This implies a “fluid” interaction with the surface. Alternatively, an elastic coupling of the cytoskeleton to the surface is an option. Most likely, some visco-elastic coupling exists. Here we chose the viscous-like adhesion for simplicity, and also because at low rates of cytoskeletal movements relative to the surface (observed in sperm cells) the viscous-like adhesion is very plausible. Thus, the cytoskeletal velocity may be calculated as:

$$v(x, t) = \frac{1}{\xi(y)} \frac{\partial \sigma}{\partial x}. \quad (5)$$

Here $\xi(y)$ [pN·s/ μm^2] is the effective drag coefficient (see Appendix B).

Boundary Conditions. The rear cytoskeletal node moves with rate $v(r(t))$, and the cytoskeletal strip at the rear depolymerizes with rate V_d . The leading node moves with velocity $v(f(t))$, and the bundle in front of it grows with rate V_p . Thus, the free boundaries of the cell are described by the equations:

$$\frac{df}{dt} = V_p(f(t)) + v(f(t)), \quad (6)$$

$$\frac{dr}{dt} = V_d + v(r(t)). \quad (7)$$

Extension at the leading edge does not touch the substratum as it expands. (Eventually it establishes adhesion.) Thus, the leading branch of the bundle is stress free. Similarly, we assume that the rear branch of the bundle does not touch the surface (the rear node disassembles before the rearmost filaments), and so there is also no stress at the rear of the cell. We assume

that all filaments at the leading edge spontaneously assemble into the bundle. These arguments allow us to formulate the following boundary conditions:

$$\sigma(f(t)) = \sigma(r(t)) = 0, \quad b(f(t)) = b_0, \quad p(f(t)) = 0. \quad (8)$$

Here $b_0 = 500$ is the given number of bundled filaments at the front. At the trailing edge, we impose no flux boundary conditions for the densities of bundled and free fibers. Note, that Eqs. (1)–(3), complemented by formulae (4) and (5), are second-order partial differential equations. The conditions of no flux for densities of bundled and free fibers, together with the conditions $b(f) = b_0$ and $p(f) = 0$, are the four boundary conditions necessary to solve Eqs. (1) and (2). The zero stress conditions at the leading and trailing edges implicitly give the boundary conditions for Eq. (3). Indeed, Eq. (4) implies that $c(f(t)) = 1/\rho$, if $\sigma(f(t)) = 0$, and $p(f(t)) = 0$. Similarly, Eq. (4) prescribes the value of c at the rear, given the values of $b(r(t))$ and $p(r(t))$.

Constitutive Relations. As explained in Appendix B, the rate of unbundling is assumed to be constant across the cell. The adhesion drag coefficient is almost a step function: it is almost constant and small beneath the cell body, and almost constant and large in the lamellipod, with a narrow transition zone just in front of the cell body (Fig. 4(a)). We model this quantitatively using function *arctan*:

$$\xi(y) = \alpha_\xi + (2\beta_\xi/\pi) \cdot \arctan(\eta(y-L)). \quad (9)$$

Similarly, we use this trigonometric function to quantify the assumed disassembly and protrusion rates. The rate of depolymerization is very small in the lamellipod, and increases in the acidic environment of the cell body:

$$\gamma_p(y) = \alpha_p - (2\beta_p/\pi) \cdot \arctan(\eta(y-L)). \quad (10)$$

The rate of MSP polymerization is given by the equation:

$$V_p = V_0 [0.5 + (1/\pi) \cdot \arctan(\eta(y-L))] \frac{L}{f(t) - r(t)}. \quad (11)$$

Here the factor in square brackets causes MSP assembly stop in the cell body. The factor given by the ratio of the cell body length to the whole cell length is due to the depletion of the membrane regulatory proteins in the longer cell. This causes slower leading edge advancement of longer cells.

Detailed explanation of these relations can be found in Appendix B. We consider the rate of the cytoskeletal disassembly at the rear, V_d , to be constant.

4. RESULTS

We solve the model equations numerically (see Appendix D) with the following initial conditions:

$$b(x, 0) = b_0, \quad c(x, 0) = 1/\rho, \quad p(x, 0) = 0$$

(Initially, there is homogeneous unstressed bundle across the cell and no individual filaments.) We varied the initial length of the cell and perturbed the initial conditions and model parameters in a number of ways. In all simulations, a unique, asymptotically stable pattern of locomotion (Figs. 3–5) evolved by the time the cell had moved a few body lengths (few tens of microns, or few minutes). Figure 3 illustrates how the lamellipodial

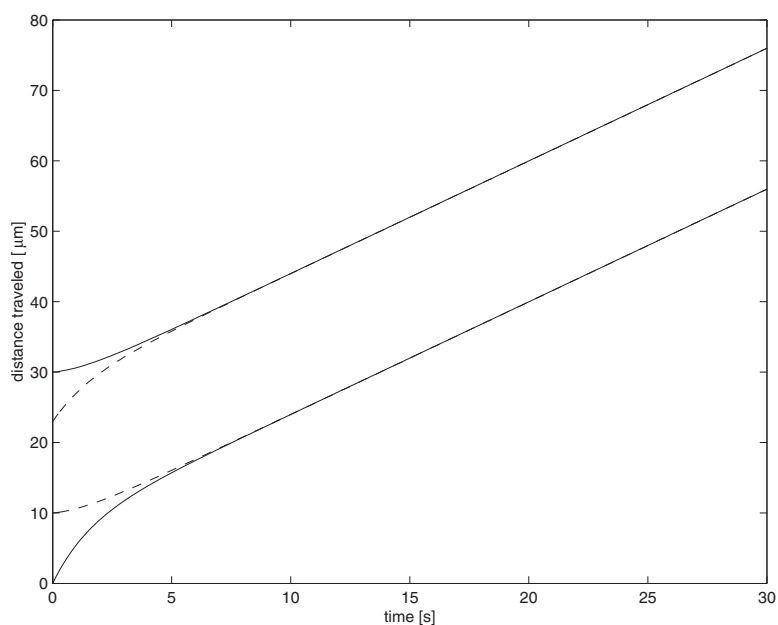


Fig. 3. Computed positions of the rear and front of the cell as functions of time. Solid and dashed curves show the trajectories of the cell's edges that evolve from different initial conditions. Asymptotically stable cell shape of length 20 μm develops, traveling steadily with velocity 1.6 $\mu\text{m/s}$.

length and migration velocity regulate to constant values. At the parameter values given in Table II, both rear and front edges of the cell advance with velocity $1.6 \mu\text{m/s}$. (In both simulations, the same initial conditions, except for the cell length, were used, see Appendix D.) The length of the cell stabilizes at $20 \mu\text{m}$, so that in our calculations, the length of the lamellipod is equal to that of the cell body. This regulation stems from a negative feedback loop: In a longer cell, the rate of protrusion is reduced, while in shorter ones this rate increases, so that protrusion and retraction are matched, corresponding to observations of living, crawling sperm.⁽⁷⁾ Velocity and size of the computational cell also compare favorably with observations.

Figure 4 shows adhesion, stress and velocity distributions across the cell. The stress is zero at the front: The bundle is not compressed, and free

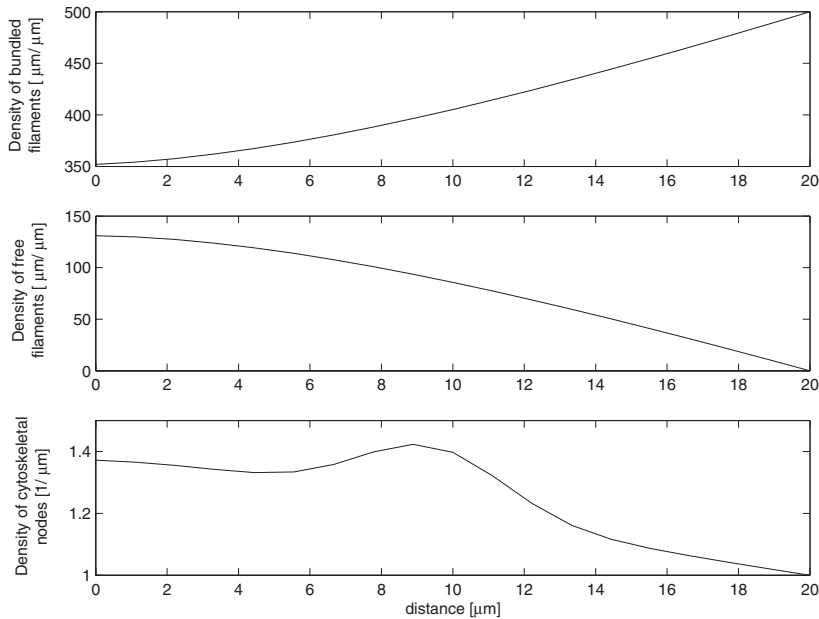


Fig. 4. Asymptotically stable stationary distributions of adhesion strength, stress, cytoskeletal velocity and drag force evolve in 10 s. Corresponding numerical solutions are shown as functions of distance from the rear edge of the cell. Top: Effective adhesion drag coefficient is almost step-like, large at the front of the lamellipod, and small at the cell body. Second from the top: Stress increases away from the front due to growing entropic forces generated by the increasing number of free filaments. Stress decreases from the middle to the rear of the cell, due to contraction of the bundle. Third from the top: The cytoskeletal velocity is negative at the front and positive at the rear due to effective filament contraction in the middle of the cell. Bottom: The drag force is negative at the front and positive at the rear.

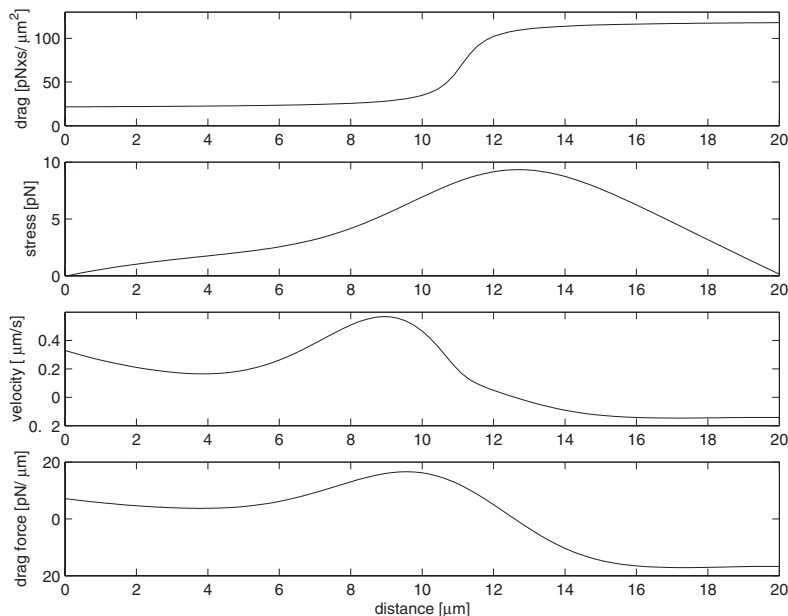


Fig. 5. Asymptotically stable stationary distributions of cytoskeletal densities evolve in 10 s. Corresponding numerical solutions are shown as functions of distance from the rear edge of the cell. Top: Density of the bundled filaments decreases away from the front due to the unbundling process. Middle: Density of the free filaments increases away from the front, because unbundling is more rapid than disassembly. Bottom: Density of cytoskeletal nodes increases under the cell body due to the contraction of the bundle. It is maximal in the middle of the cell, where the contraction is maximal.

filaments are absent. As the unbundling process takes place across the lamellipod, increasing numbers of free individual polymers in tension try to contract. This increases the stress toward the middle of the cell and compresses the bundle. The velocity of the cytoskeleton is low at the front due to strong adhesion. In the middle of the cell, just ahead of the cell body, where adhesion decreases rapidly, developing stress causes the velocity of cytoskeletal elements to increase. The cytoskeleton contracts, relieving the stress toward the rear of the cell. The contraction in the middle of the cell pulls the cell body forward and moves the lamellipod backward. Because of the graded character of adhesion, retrograde flow of the lamellipod is slow ($-0.15 \mu\text{m/s}$), while the cell body advances at $1.6 \mu\text{m/s}$. The MSP filaments at the front assemble with rate $1.75 \mu\text{m/s}$, so that the rate of protrusion, $(1.75 - 0.15 \mu\text{m/s})$ is equal to the rate of depolymerization plus the rate of retraction at the rear of the cell $(1.25 + 0.35 \mu\text{m/s})$.

The magnitude of the drag force is maximal at the leading edge. This does not agree with calculations in ref. 10. The reason is that in ref. 10 the lamellipodial cytoskeleton was considered to be much less stiff, and that the 2-D area of the lamellipod was much greater, than that of the cell body. Note, that the total drag force integrated across the cell, which is just the derivative of the stress, is equal to zero, because the stress is zero at both edges.

Figure 5 shows stationary distributions of the cytoskeletal elements involved. The density of bundled filaments decreases from the front to the rear of the cell due to the unbundling process. Conversely, the density of free individual filaments increases toward the rear, because unbundling occurs more rapidly than disassembly of the polymers. At the given values of the model parameters, a significant number of filaments are bundled throughout the cell, and the overall bundle is sufficiently rigid everywhere. Therefore, even though contractile stress developing in the middle of the cell is significant, the actual contraction of the cytoskeleton is small. The distance between cytoskeletal nodes decreases toward the rear (or equivalently, node density increases) insignificantly.

Note, that in the evolved stationary state, the flux of the cytoskeletal nodes has to be constant in the frame of the steadily moving cell: $(v(x-Vt)-V)c(x-Vt) = \text{const}$. Here V is the equal rates of advancement of the cell edges: $V = V_d + v(r(t)) = V_p + v(f(t))$. Note, that from these two expressions, the third one easily follows: $V_d c(r(t)) = V_p c(f(t))$, which means that the rate of the nodes assembly at the front is equal to their rate of disassembly at the rear. Numerical solutions validate all these relations. Implicitly, these relations determine the cell length and rate of movement in a unique way.

5. DISCUSSION

We constructed a simple one-dimensional physical model of the MSP fiber complex stretching in the anterior–posterior direction across the motile cell. This complex consists of filaments that assemble and bundle at the front, un-bundle and disassemble at the rear and adhere to the surface at the front and middle. The resulting treadmilling process generates the cell locomotion. The spatial separation of protrusion, contraction and adhesion is maintained by the pH gradient, which develops from the source of protons in the cell body and transmembrane leakage of protons. A central feature of the model is the energy turnover pathway in the locomotive cell. Flexible coiled MSP filaments assemble at the leading edge and aggregate into a tight bundle. During this process, thermal writhing of the filaments is ratcheted by the binding of the filaments to the bundle. This

ratchet mechanism generates the force of protrusion, at the same time locking filaments into an elongated configuration, and storing elastic energy. This stored energy is subsequently released as filaments dissociate from the bundle at the rear of the lamellipod, contracting from their stretched configuration into their coiled state. The resulting entropic force pulls the cell body forward.

The model accounts for the observed steady, stable movement of the nematode sperm. The model could be used to analyze some future experiments. An analysis of the traction forces is not likely to be very informative because of the importance of the behavior at the lateral edges of the cell, which our 1-D model ignores. However, the experiments with changing external pH and subsequent disruption of the steady locomotion could be compared with the corresponding model behavior. Also, sometime the migrating cells get “tethered:” one of the attachment sites get stabilized and keeps the cell from moving away. In this situation, the cytoskeleton starts to treadmill, while the cell shape changes. When more accurate measurements of this phenomenon are available, one can simulate it by changing the adhesion function $\zeta(y)$. In addition to providing a physical basis for the amoeboid motility of the nematode sperm, our model also may be useful in elucidating actin-based cell locomotion.

Mathematically, the questions about existence (in certain space) and uniqueness of the stationary solutions of the model equations, as well as about stability of these stationary states, remain open. In this paper, we restrict ourselves to the numerical analysis that demonstrates that the same profiles of densities, velocities and forces evolve on the domain of the same length moving with the same rate when number of different initial conditions are used. More rigorous analysis is prohibitive due to complex nature of our nonlinear free boundary problem. There are no general stability techniques applicable to our model (like those for travelling wave solutions on the real line, i.e., Kolmogoroff analysis of Fisher equation).⁽¹³⁾ A mathematically similar, yet simpler, model of autophobic spreading of drops was treated at higher level of mathematical sophistication, than that in our paper.⁽¹⁴⁾ Neither stability, nor uniqueness of the stationary solutions were proved there.

The model has significant limitations. Due to its one-dimensional character, it cannot capture important processes at the lateral sides of the cell which stabilize cell shape.⁽¹⁰⁾ The model also ignores complex physical effects that stem from the fact that MSP gel and lamellipodial cytoplasm are polyelectrolytes. For simplicity, movement of aqueous parts of the lamellipodial cytoplasm were not considered in this paper. Corresponding phenomena will be treated elsewhere.⁽¹⁵⁾ In general, the “push-pull” model, even treated quantitatively, is only a very plausible explanation of the

biological phenomenon. First, a partial explanation for the apparent simplicity of the nematode sperm cytoskeleton is that the amount of research on the actin cytoskeleton is much greater than that spent studying MSP based cytoskeletons. Second, the picture of the cytoskeleton as a stable, well organized scaffold, which the model is based on, is oversimplified. Some polymerization and depolymerization take place across the whole lamellipod, as well as more complex processes of severing and annealing of MSP filaments. Also, angular order in the cytoskeleton has not been studied. The orderliness of the cytoskeleton is an assumption of the model, which will have to be tested in the future. More experimental and theoretical research will be required to validate our theory. Since current knowledge regarding the molecular biology of the nematode sperm cell is limited, some model assumptions and parameter values cannot be linked directly to experimental data. Because of these limitations, the model provides only conceptual conclusions about cell motility, rather than making specific testable predictions. Nevertheless, the strength of this model is that, like the experimental studies, it helps to dissect the complex phenomenon of cell migration.

APPENDIX A: PROTRUSION

Thermal motion of the growing filament tip is equivalent to a biased random walk.⁽¹¹⁾ The tip is “locked” every time its length increases on δ , where δ is the distance between neighboring adhesive patches. This process is equivalent to the *polymerization ratchet*.⁽¹⁶⁾ According to the general theory of the polymerization ratchet, this mechanism generates a force of the order of $k_B T / \delta$. The reasonable estimate is $\delta \sim 10 - 40$ nm. Then, one filament generates a force $\sim 0.1 - 0.4$ pN. There are ~ 500 filaments in the bundle. Assuming that protrusion forces are additive,⁽¹⁷⁾ the total force is ~ 100 pN. There is no direct data about the sperm cell membrane tension. Using scarce data related to the lipid bilayer⁽¹⁷⁾ (tens of pN per μm at the leading edge), and taking into account that there is one bundle per μm at the leading edge, we conclude that the force of the “bundling ratchet” is sufficient to drive protrusion. In the model, we assume that the membrane resistance is much less than the stall force of the ratchet, and that bundle growth at the leading edge is load-free.

Two factors determine the velocity of protrusion, V_p : The rate of the bundling ratchet, and the polymerization velocity. The order of magnitude of the former is D/δ , where $D \sim 10^7$ nm²/s is the effective diffusion coefficient describing thermal writhing of a filament tip $\sim 10 - 40$ nm long.⁽¹⁸⁾ The corresponding velocity, $\sim 10^3$ $\mu\text{m}/\text{s}$, cannot limit the observed, much

smaller, protrusion rate. Thus, in the model we assume that the polymerization velocity of MSP filaments, V_p , is the rate of advancement of the leading edge.

APPENDIX B: PH DISTRIBUTION

We model the proton distribution on the 1-D lamellipodial domain by the reaction-diffusion equation:

$$\frac{\partial h}{\partial t} = D \frac{\partial^2 h}{\partial x^2} - \lambda(h - h_{\text{ext}}), \quad r(t) + L_{\text{cb}} < x < f(t).$$

Here, $h(x, t)$ is the proton concentration, D is the proton diffusion coefficient in the cytoplasm, λ is the proton leakage rate across the cell membrane, and h_{ext} is the proton concentration outside the cell. We assume that the proton concentration across the cell body is constant: $h(x) = h_0$ at $r(t) < x < r(t) + L_{\text{cb}}$. We impose the no flux boundary condition at $x = f(t)$, assuming that the proton leakage through the thin leading edge is negligible in comparison with that through the broad and flat lamellipodial membrane. The diffusion of protons is very fast, and proton concentration relaxes to its steady state rapidly relative to the time scale of cell motion. This allows us to scale-out temporal dynamics of the proton distribution and to describe proton concentration by the Helmholtz equation:

$$D \frac{d^2 h}{dx^2} - \lambda(h - h_{\text{ext}}) = 0, \quad h(r + L_{\text{cb}}) = h_0, \quad \left. \frac{dh}{dx} \right|_{x=f} = 0.$$

Solution of this equation can be found analytically:

$$h(x) = h_{\text{ext}} + A \cosh(\tilde{\lambda}(x - f)), \quad A = \frac{h_0 - h_{\text{ext}}}{\cosh(\tilde{\lambda}(f - r - L_{\text{cb}}))}, \quad \tilde{\lambda} = \sqrt{\lambda/D}.$$

In the zeroth approximation, proton distribution decreases exponentially in the forward direction:

$$h(x) \simeq h_{\text{ext}} + (h_0 - h_{\text{ext}}) \exp[-\tilde{\lambda}(x - r - L_{\text{cb}})]. \quad (12)$$

Equivalently, pH distribution increases linearly with distance from the cell body.

We assume that assembly rate, depolymerization rate and adhesion strength are functions of pH, proportional to the expression $\arctan(\tilde{\eta}(\text{pH}(x) - \text{pH}_c))$, where $\tilde{\eta}$ and pH_c are constants. This means that the corresponding rates change when $\text{pH} \simeq \text{pH}_c$; Parameter $\tilde{\eta}$ determines a pH interval,

wherein changes take place. According to Eqs. (9)–(11), this is equivalent to the statement that the assembly rate, depolymerization rate and adhesion strength are functions of spatial coordinate, proportional to the expression $\arctan(\eta(y-L))$, where $y = x - r$, and L and η are model parameters. $L - L_{cb}$ is the distance from the cell body to where pH drops to its critical value pH_c . We assume that $L - L_{cb} = 1 \mu\text{m}$, so $L = 11 \mu\text{m}$, and that $\eta = 1/\mu\text{m}$.

Specific forms of the assembly rate, depolymerization rate and adhesion strength are given by Eqs. (9)–(11). We assume that the rate of unbundling rate is constant and independent of pH. Finally, the MSP assembly rate, besides pH, is limited by the concentration of membrane protein, which activates MSP dimers and makes them able to polymerize. If the total number of such proteins is constant, then their concentration is inversely proportional to cell length, assuming that these proteins diffuse rapidly throughout the membrane. This explains the last factor in (11).

APPENDIX C: ESTIMATES OF THE MODEL PARAMETERS AND SCALES

Values for model parameters are given in Table II. The order of magnitude of cell body length, L_{cb} and MSP assembly rate, V_0 , are available from observations. We choose the values of L and η based on the observation that disassembly and adhesion change their patterns 1–2 μm in front of the cell body, and that this change occurs over a zone in μm range. The rate of unbundling, γ_b , is chosen to reflect observations that the thickness of MSP fiber complexes changes significantly, but not orders of magnitude, over the cell length. Rates of depolymerization, unavailable from experiment, are adjusted so that the number of free filaments is comparable with that of the bundled filaments, and so that the polymers do not pile up at the rear of the cell. The order of magnitude of the adhesion drag coefficient is also unknown; we use the estimate of ref. 10 adjusted to a one-dimensional situation.

Without loss of generality, we assume that the distance between cytoskeletal nodes at the front, and thus the rest length of the effective spring associated with the bundle, $\rho = 1 \mu\text{m}$. Furthermore, we use the characteristic spring constant of a globular protein, $\sim 1 \text{ pN/nm}$, to describe an MSP dimer. Assuming that a bundled filament of length 1 μm is equivalent to ~ 1000 springs in series (the size of the MSP dimer is in nm range), the spring constant per one bundled filament can be estimated as $K = 1 \text{ pN}/\mu\text{m}$. The effective spring constant corresponding to an unbundled individual filament is equal to $\kappa = (3k_B T)/(l_p l)$,⁽¹¹⁾ where l_p is the persistence length of MSP filaments, and l is their average contour length.

Filaments are very flexible, and we assume that their persistence length, $l_p \sim 0.01 \mu\text{m}$, is much less, than their contour length, $l \sim 1 \mu\text{m}$. Then, $\kappa \sim 1 \text{ pN}/\mu\text{m}$.

We non-dimensionalize the model using the time scale $\bar{T} = 40 \text{ s}$, the characteristic time interval for the cell to travel few cell lengths, and the spatial scale $\bar{L} = 10 \mu\text{m}$, the length of the cell body. We also use $\bar{F} = 10 \text{ pN}$, the characteristic magnitude of contractile stress, as the scale of force. All parameters are given in physical and dimensionless units in Table II. Dimensionless parameters were used in numerical simulations.

APPENDIX D: NUMERICAL ANALYSIS

Equations (1)–(5) and (8)–(11) were integrated using Lax–Friedrich finite difference scheme⁽¹⁹⁾ on a constant grid with the spatial step equal to 0.025 (0.25 μm). We chose the time step small enough to maintain stability, but not too small (close to the stability limit) in order not to introduce large errors. In the simulations shown here, the initial conditions reported in Section 4 were used. To investigate the stability of the evolving solutions, we added small random components to these initial conditions. Equations (6) and (7) were integrated using forward Euler method. At each step, we identified the discrete cell boundary as grid points closest to respective continuous solutions of Eqs. (6) and (7). The numerical simulations were performed on a PC using Matlab. Computations necessary to simulate the cell for 4–5 time units (160–200 s) took a few hours.

ACKNOWLEDGMENTS

We thank G. Oster, C. Wolgemuth and B. Slepchenko for useful discussions. A.M. is supported by a UCD Chancellor's Fellowship, NSF Grant DMS-1097746 and an NIH Grant "Cell Migration Consortium" NIGMS U54 GM64346. D.V. was supported by RTG NSF Grant DBI-9602226 "NonlineardynamicsinBiology" at the Institute for Theoretical Dynamics; and is supported in part by the San Diego State University Foundation.

REFERENCES

1. D. Bray, *Cell Movements: From Molecules to Motility* (Garland Publ., New York, 2001).
2. M. Dembo and Y.-L. Wang, Stresses at the cell-to-substrate interface during locomotion of fibroblasts, *Biophys J.* **76**:2307–16 (1999).
3. M. Abercrombie, The Croonian lecture: The crawling movement of metazoan cells, *Proc. Roy. Soc. London Ser. B* **207**:129–147 (1980).
4. T. J. Mitchison and L. P. Cramer, Actin-based cell motility and cell locomotion, *Cell* **84**:371–379 (1996).

5. G. G. Borisy and T. M. Svitkina, Actin machinery: Pushing the envelope, *Curr. Opin. Cell Biol.* **12**:104–12 (2000).
6. A. B. Verkhovsky, T. M. Svitkina, and G. G. Borisy, Network contraction model for cell translocation and retrograde flow, *Biochem. Soc. Symp.* **65**:207–222 (1999).
7. T. Roberts and M. Stewart, Acting like actin: The dynamics of the nematode major sperm protein (MSP) cytoskeleton indicate a push-pull mechanism for amoeboid cell motility, *J. Cell Biol.* **149**:7–12 (2000).
8. J. Italiano, M. Stewart, and T. Roberts, Localized depolymerization of the major sperm protein cytoskeleton correlates with the forward movement of the cell body in the amoeboid movement of nematode sperm, *J. Cell Biol.* **146**:1087–1095 (1999).
9. J. Italiano, T. Roberts, M. Stewart, and C. Fontana, Reconstitution in vitro of the motile apparatus from the amoeboid sperm of ascaris shows that filament assembly and bundling move membranes, *Cell* **84**:105–114 (1996).
10. D. Bottino, A. Mogilner, T. Roberts, M. Stewart, and G. Oster, How nematode sperm crawl, *J. Cell Science* **115**:431–453 (2002).
11. M. Doi, *Introduction to Polymer Physics* (Clarendon Press, Oxford, 1996).
12. L. Landau and E. Lifshitz, *Theory of Elasticity* (Butterworth-Heinemann, Boston, 1995).
13. J. D. Murray, *Mathematical Biology* (Springer, New York, 1989).
14. J. K. Hunter, Z. Li, and H. Zhao, Reactive autophobic spreading of drops, *J. Comput. Phys.* In Press (2002).
15. C. W. Wolgemuth, A. Mogilner, and G. Oster, The hydration dynamics of polyelectrolyte gels with applications to drug delivery and cell motility, *Biophys. J.*, Submitted.
16. A. Mogilner, T. Elston, H.-Y. Wang, and G. Oster, Molecular motors, in *Joel Keizer's Computational Cell Biology*, C. P. Fall, E. Marland, J. Tyson, and J. Wagner, eds. (Springer, New York, 2002), pp. 321–380.
17. A. Mogilner and G. Oster, The physics of lamellipodial protrusion, *Eur. Biophys. J.* **25**:47–53 (1996).
18. A. Mogilner and G. Oster, Cell motility driven by actin polymerization, *Biophys. J.* **71**:3030–3045 (1996).
19. R. J. LeVeque, *Numerical Methods for Conservation Laws* (Birkhauser, Boston, 1992).